


RESEARCH

Open Access



Impaired glymphatic function in the early stages of disease in a TDP-43 mouse model of amyotrophic lateral sclerosis

Akram Zamani¹, Adam K. Walker², Ben Rollo¹, Katie L. Ayers^{3,4}, Raysha Farah¹, Terence J. O'Brien^{1,5} and David K. Wright^{1*} 

Abstract

Background: Multiple lines of evidence suggest possible impairment of the glymphatic system in amyotrophic lateral sclerosis (ALS). To investigate this, we used *in vivo* magnetic resonance imaging (MRI) to assess glymphatic function early in the course of disease in a transgenic mouse with doxycycline (Dox)-controlled expression of cytoplasmic human TDP-43 (hTDP-43ΔNLS), mimicking the key pathology implicated in ALS.

Methods: Adult TDP-43 transgenic and littermate monogenic control mice underwent longitudinal multimodal MRI one and three weeks after the cessation of Dox feed, together with weekly rotarod assessments of motor performance. Glymphatic function was assessed using dynamic contrast-enhanced MRI to track the clearance of an MR contrast agent injected into the cisterna magna.

Results: Compared to their littermate controls, TDP-43 mice exhibited progressive neurodegeneration including that within the primary motor cortex, primary somatosensory cortex and corticospinal tract, significant weight loss including gastrocnemius atrophy, and shortened telomere length. Furthermore, in the presence of this ALS-like phenotype, these mice have significantly disrupted glymphatic function.

Conclusions: Although the relationship between glymphatic clearance and ALS disease progression remains to be elucidated, these changes occurred very early in the disease course. This provides initial evidence to suggest that the glymphatic system might be a potential therapeutic target in the treatment of ALS.

Keywords: Magnetic resonance imaging, Diffusion-weighted imaging, Neurodegeneration, Cerebrospinal fluid, Telomere

Background

Neurodegenerative diseases are chronic and inexorable conditions characterized by the presence of insoluble aggregates of abnormally ubiquitinated and phosphorylated proteins [1]. Transactive response DNA-binding protein 43 (TDP-43) is one such protein implicated in the neurodegenerative process and the presence of TDP-43

inclusions in neurons is a hallmark finding in amyotrophic lateral sclerosis (ALS) [2, 3]. Recent evidence also points to a prion-like self-propagation of TDP-43 misfolding, either by the circulatory system, cell-to-cell contact, or via the interstitial or cerebrospinal fluids (CSF) [1, 4–6]. As protein aggregation occurs before the onset of brain damage and motor symptoms, new therapeutic strategies targeting the spread of disease across the brain (including eliminating seed proteins and blocking cell-to-cell spread) are of vital importance.

*Correspondence: david.wright@monash.edu

¹ Department of Neuroscience, Central Clinical School, Monash University, Melbourne, VIC 3004, Australia

Full list of author information is available at the end of the article



One potential therapeutic target is the glymphatic system, a CSF-based waste clearance system for the brain [7]. Mediated by a unique system of astrocyte-specific aquaporin-4 water channels, the glymphatic system is largely dormant during wakefulness but highly active during sleep, working to clear waste byproducts from the brain through the flow of CSF [7]. Preclinical studies have shown that amyloid- β , a protein implicated in neurodegenerative diseases including Alzheimer's disease, is cleared from the brain by the glymphatic system [7] and that in aged mice, amyloid- β clearance is dramatically slowed [8]. As the prevalence of ALS also increases with age, sleep disturbances are exceedingly common in ALS [9] and given that a single night of sleep deprivation can result in amyloid- β accumulation linked with Alzheimer's disease [10], we hypothesize that glymphatic clearance is also impaired in ALS.

To investigate this, we assessed glymphatic function in a TDP-43 transgenic mouse model of ALS. Specifically, these mice have doxycycline (Dox)-suppressible neurofilament heavy chain (*NEFH*) promoter-driven expression of human TDP-43 (hTDP-43) harboring a defective nuclear localization signal (hTDP-43 Δ NLS). When these mice are removed from Dox feed, hTDP-43 becomes expressed, resulting in the accumulation of insoluble phosphorylated cytoplasmic TDP-43 in neurons of the brain and spinal cord and loss of endogenous nuclear mouse TDP-43 [11]. Continued hTDP-43 expression has been shown to result in much of the pathophysiology seen in ALS, including brain atrophy, cortical and spinal motor neuron loss, muscle denervation, and progressive motor impairments, leading to premature death.

We performed longitudinal multimodal magnetic resonance imaging (MRI) one and three weeks after the cessation of Dox feed, together with weekly rotarod assessments of motor performance. Glymphatic function was assessed using dynamic contrast-enhanced MRI (DCE-MRI) to track the clearance of an MR contrast agent injected into the cisterna magna [12]. DCE-MRI was performed following the second multimodal imaging session three weeks after the cessation of Dox feed.

Methods

Animals

This study included 7 NEFH+/NLS+(rNLS8) double transgenic mice with Dox-suppressible expression of hTDP-43 Δ NLS (referred to as 'TDP-43 mice' throughout) and 5 NEFH-/NLS+ single transgenic littermate controls (Jackson Laboratories, *NEFH-tTA* line 8, stock #025,397 and *tetO-TARDBP** line 4, stock #014,650), on a pure C57Bl/6Jausb background following ~10 generations of backcrossing. The phenotypes of these mice were consistent with that described in detail previously

[11]. Mice were all males, aged 10–12 weeks and group-housed under a 12 h/12 h light/dark cycle with ad libitum access to food and water. All of the 12 mice were provided with 200 mg/kg Dox-containing chow (Diet SF11-059, Specialty Feeds, Glen Forrest, Western Australia, Australia) until the start of their experimental paradigm when they were switched to standard chow.

Experimental design

Mice were placed on standard chow for three weeks, by which time the TDP-43 mice are expected to demonstrate decreased body mass, hindlimb clamping and sensorimotor deficits [11]. The mice underwent weekly behavioral testing and in vivo MRI at 1 and 3 weeks after the cessation of Dox feed. DCE-MRI was performed following the second MRI at three weeks after the cessation of Dox feed, to assess glymphatic function. At the end of the DCE-MRI imaging session, the mice were deeply anaesthetized with an intraperitoneal injection of sodium pentobarbital (Lethobarb, Virbac, Australia). A sample of ear tissue was collected and stored at -80°C . Gastrocnemius muscles and spleens were collected and weighed.

Behavioral testing

An accelerating rotarod test was performed to assess sensorimotor coordination, balance and stamina. Mice were placed on a rotating cylinder with 3-cm diameter (Rotarod-RS; Panlab, Harvard Bioscience, Holliston, MA) that accelerated by 1 rpm every 8 s from an initial speed of 5 rpm. The cylinder continued to accelerate until the mouse fell off. The test was repeated three times at 10-min intervals. The latency to fall was recorded for each test and the average of all three tests was reported. Following the rotarod test, the mice were assessed for hindlimb clamping as described previously [11]. Behavioral assessments were performed during the light cycle at 1, 2 and 3 weeks after cessation of Dox feed.

MRI

In vivo imaging was performed with a 9.4 T Bruker MRI, at 1 and 3 weeks after cessation of Dox feed, and included T_2^* -weighted and diffusion-weighted imaging (DWI) acquisitions. Mice were anesthetized using isoflurane in a carrier gas of 100% oxygen with body temperature maintained using a hot water system. Depth of anesthesia was monitored by measuring the respiration rate with a pressure-sensitive pillow positioned under the diaphragm (SA Instruments Inc., Stony Brook, NY). 3D T_2^* -weighted images were acquired in the axial plane with a multi-gradient echo sequence and parameters: repetition time (TR)=70 ms; echo time (TE)=2 ms; echo spacing=3 ms; 10 echoes; field of view (FOV)= $16 \times 16 \times 8 \text{ mm}^3$; and isotropic resolution= $125 \times 125 \times 125 \text{ }\mu\text{m}^3$.

DWI was acquired in ~10 min using a single-shot 2D diffusion tensor imaging (DTI)-echo planar imaging sequence. Two b_0 images and two diffusion shells (b -value = 1500 s/mm² and 3000 s/mm²) were acquired with 81 directions, δ = 3.5 ms and Δ = 12 ms. Other imaging parameters were adjusted to give an isotropic resolution of 250 μ m³ and included: TR = 3600 ms; TE = 25 ms; and FOV = 16 × 16 mm².

At 3 weeks post-Dox, *in vivo* DCE-MRI was also performed. A baseline DCE-MRI scan was acquired over the whole-brain using a 3D FLASH sequence with the following imaging parameters: TR = 12 ms; TE = 2.1 ms; flip angle = 15°; FOV = 19.2 × 19.2 × 14.4 mm³; matrix = 128 × 128 × 96; resolution = 150 × 150 × 150 μ m³; and number of excitations = 2.

The mouse was then withdrawn from the magnet and the cisterna magna cannulated using a 30G needle, connected to polyethylene tubing (BPTE-10, Instech Laboratories Inc., Plymouth Meeting, PA) filled with Magnevist (gadopentetate dimeglumine; Bayer AG, Berlin, Germany) [33]. Ten microlitres of Magnevist (20 mM) was infused over 10 min using a perfusion pump and a Hamilton syringe. The needle was left in place for 5 min after infusion, then slowly withdrawn. The mouse was repositioned inside the MRI scanner and DCE-MRI imaging resumed 30 min after the start of the infusion, with T₁-weighted images acquired every 5 min for 170 min. Isoflurane anesthesia was maintained throughout the imaging process.

MRI analysis

The T₂*-weighted images were registered to the Waxholm Space adult C57BL/6 J mouse brain atlas using symmetric diffeomorphic normalization. The inverse diffeomorphisms were then used to register the atlas labels to native space. Volumes were calculated for four regions of interest (ROIs), including the whole brain, neocortex, hippocampus and hypothalamus. Additionally, whole-brain tensor-based morphometry analysis was performed on smoothed log-Jacobian images calculated from the diffeomorphisms as described previously [13].

DWI processing was performed with the MRtrix3 [14] and FSL packages and included denoising, Gibbs correction and eddy current correction followed by a fully automated estimation of three tissue response functions. Fibre orientation distributions were estimated using multi-tissue constrained spherical deconvolution and normalized, and a study-specific template was generated for statistical analysis of the fixel-based metric fibre density and cross-section (FDC) [15]. To assess any differences in microstructural changes in TDP-43 and control mice over time, the week-3 fixel values were subtracted

from week-1 fixel values, and statistical testing performed on the delta values (Δ FDC).

An a priori analysis of the corticospinal tracts was also performed. Left and right corticospinal tract streamlines were segmented as described previously [13]. The segmented streamlines were used to identify the corticospinal tract fixels, i.e. those fixels aligned parallel to the streamlines of interest—and the maximum FDC value was calculated for each voxel. FDC values were then sampled along the corticospinal tracts at 20 equidistant sections from the pons to the motor cortex.

To correct for movement over time, DCE-MRI T₁-weighted images were aligned using a rigid transform. A mapping between the mean T₁-weighted image and the Waxholm Space adult C57BL/6 J mouse brain atlas, down sampled to 43 × 43 × 43 μ m³, was generated using symmetric image normalization and the atlas segmentations transformed into T₁-weighted image space. The average signal increase over baseline was calculated at each time point using MATLAB for 6 atlas-defined ROIs: the whole brain, excluding the ventricles; pons; amygdala; olfactory bulb; thalamus; and cerebellum.

Telomere analysis

DNA extraction from 25-mg ear tissue was performed using DNeasy® Blood and Tissue kit (QIAGEN, Hilden, Germany) according to the manufacturer's instructions. The quality and quantity of DNA was measured using the QIAxpert system and samples with an A260/A280 ratio of 1.7–2 were used. DNA was diluted to 20 ng/ μ l in Tris-EDTA buffer solution for further analysis. Two master mixes containing telomere repeat copy and a single copy gene (36B4) were used. The qPCR mix contained 1 μ l DNA, 1 × SYBR Green master mix (Promega, Madison, WI), and forward and reverse primers. The final primer concentrations were as follows: telomere forward 270 nM, telomere reverse 900 nM, 36B4 forward 300 nM and 36B4 reverse 500 nM.

Auto-aliquoting was performed using the QIAgility liquid handling robot and samples were run in duplicates with primer sequences as described previously [16]. The thermocycling conditions for telomere were 1 cycle at 95 °C for 3 min, 30 cycles of 95 °C for 15 s and 54.8 °C for 1 min followed by the melting curve, and for 36B4 were 1 cycle at 95 °C for 3 min, 30 cycles of 95 °C for 15 s and 58.4 °C for 1 min followed by the melting curve. Telomere length was determined by comparing telomere to 36B4 as described previously [17].

Statistical analyses

Voxel-wise analysis of tensor-based morphometry was performed using the FSL's Randomise with threshold-free cluster enhancement [18], and results were fully

corrected for multiple comparisons. Changes in Δ FDC were assessed using connectivity-based fixel enhancement with results fully corrected for family-wise error (FWE). Corticospinal tract analyses of FDC were tested using a general linear model with time as repeated measure (1 and 3 weeks post-Dox) and genotype (TDP-43, control) and position along the tracts (p1 to p20) as factors. Statistical testing was performed using the IBM SPSS Statistics for Macintosh, Version 27.0.

Two-way ANOVAs or mixed-effects analyses with genotype (TDP-43 vs control) as the between-subject factor and time (1 week vs 3 weeks post-Dox) as the within-subject factor were used to assess behavior and ROI-based measures. Šídák's multiple comparison tests were performed where necessary. Data on telomere length were analyzed with an unpaired *t*-test. Statistical testing for these comparisons was performed using GraphPad Prism version 9.1.0 software (GraphPad, San Diego, CA). Significance for all tests was set at $P < 0.05$ and all results are presented as mean \pm standard error of the mean (SEM).

Results

TDP-43 mice exhibited ALS-like phenotype with symptoms deteriorating over time

To determine if TDP-43 mice develop a progressive motor phenotype, we assessed motor coordination, balance and stamina using the rotarod test at 1, 2 and 3 weeks after the cessation of Dox feed. Two-way ANOVA revealed a significant interaction between time and genotype ($F_{2,20} = 27.05$, $P < 0.0001$), with control mice running for significantly longer than TDP-43 mice ($F_{1,10} = 99.74$, $P < 0.0001$) and improving over time (Fig. 1a). Šídák's multiple comparisons test revealed that the TDP-43 mice performed significantly different from

control mice at all time points after cessation of the Dox feed.

Hindlimb claspings is a well-established marker for neurodegenerative disease progression [2, 11, 19] and we found that the TDP-43 mice also developed early-onset hindlimb claspings over time (Fig. 1b). While none of the control mice presented with hindlimb claspings during the study, 57% of the TDP-43 mice demonstrated hindlimb claspings at 1 week post-Dox feed, with the remainder being symptomatic at 2 weeks post-Dox. The TDP-43 mice also demonstrated significant body weight loss compared to the control mice (Fig. 1c). Two-way ANOVA revealed a significant interaction between time and mouse genotype ($F_{2,20} = 14.66$, $P < 0.0001$), with the TDP-43 mice having significantly lower body weight beginning from 15 days after cessation of the Dox feed.

Structural imaging revealed progressive atrophy of the grey matter in TDP-43 mice

To understand the timing and pattern of possible morphological brain changes in TDP-43 mice, we analyzed structural images using tensor-based morphometry at 1 and 3 weeks after cessation of the Dox feed. This exploratory method revealed foci of significant atrophy in TDP-43 mice compared to control mice at the latter time point (Fig. 2a). The affected regions included, from anterior to posterior, the olfactory bulb, frontal association cortex, lateral and dorsolateral orbital cortex, agranular insular cortex, globus pallidus, hippocampus, dorsal subiculum, secondary visual cortex and cerebellum. No foci of hypertrophy were detected. No atrophy or hypertrophy was detected at 1 week after cessation of the Dox feed. Interestingly, no foci of atrophy were detected in the primary motor cortex.

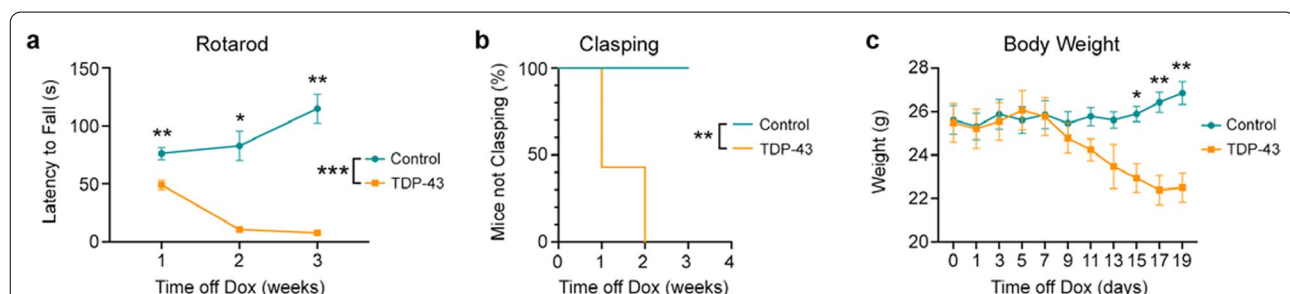
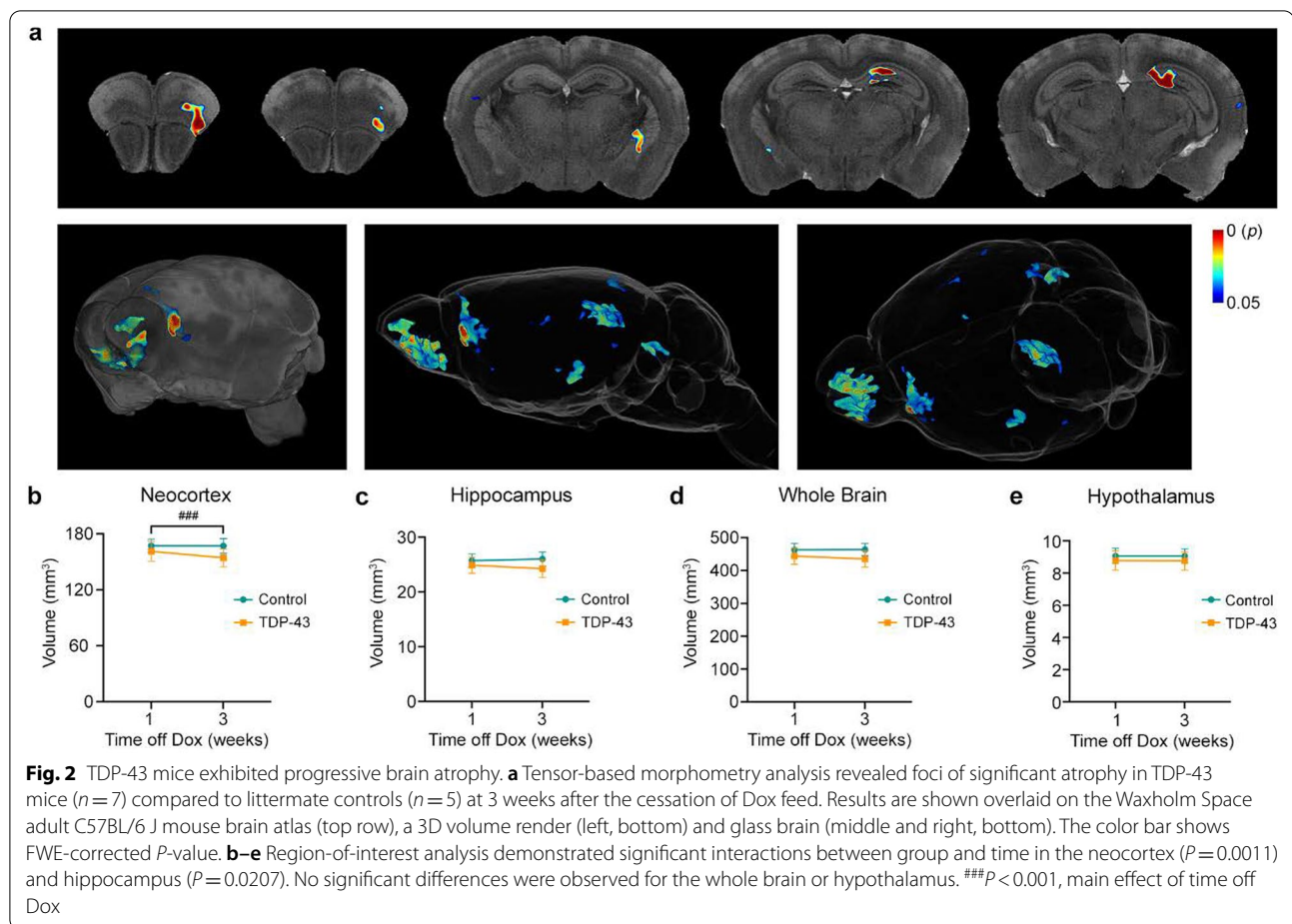


Fig. 1 Motor performance is impaired in TDP-43 mice. **a** TDP-43 mice ($n = 7$) performed significantly worse in the rotarod task than their littermate controls ($n = 5$), which improved over time. Two-way ANOVA revealed a significant interaction between time and genotype ($P < 0.0001$), and a main effect of genotype with control mice running for significantly longer than TDP-43 mice ($P < 0.0001$). **b** Survival plot showing the percentage of mice not clapping at 1, 2 and 3 weeks post-Dox cessation. **c** The body weight of mice measured on the day of, and every two days after, the cessation of Dox feed. Two-way ANOVA demonstrated a significant interaction between genotype and time ($P < 0.0001$). Main effects of genotype are indicated by lines with asterisk between genotype symbols in figure legends. Significant results following Šídák's multiple comparison testing are indicated by asterisk(s) at corresponding time points. * $P < 0.05$, ** $P < 0.01$, *** $P < 0.001$



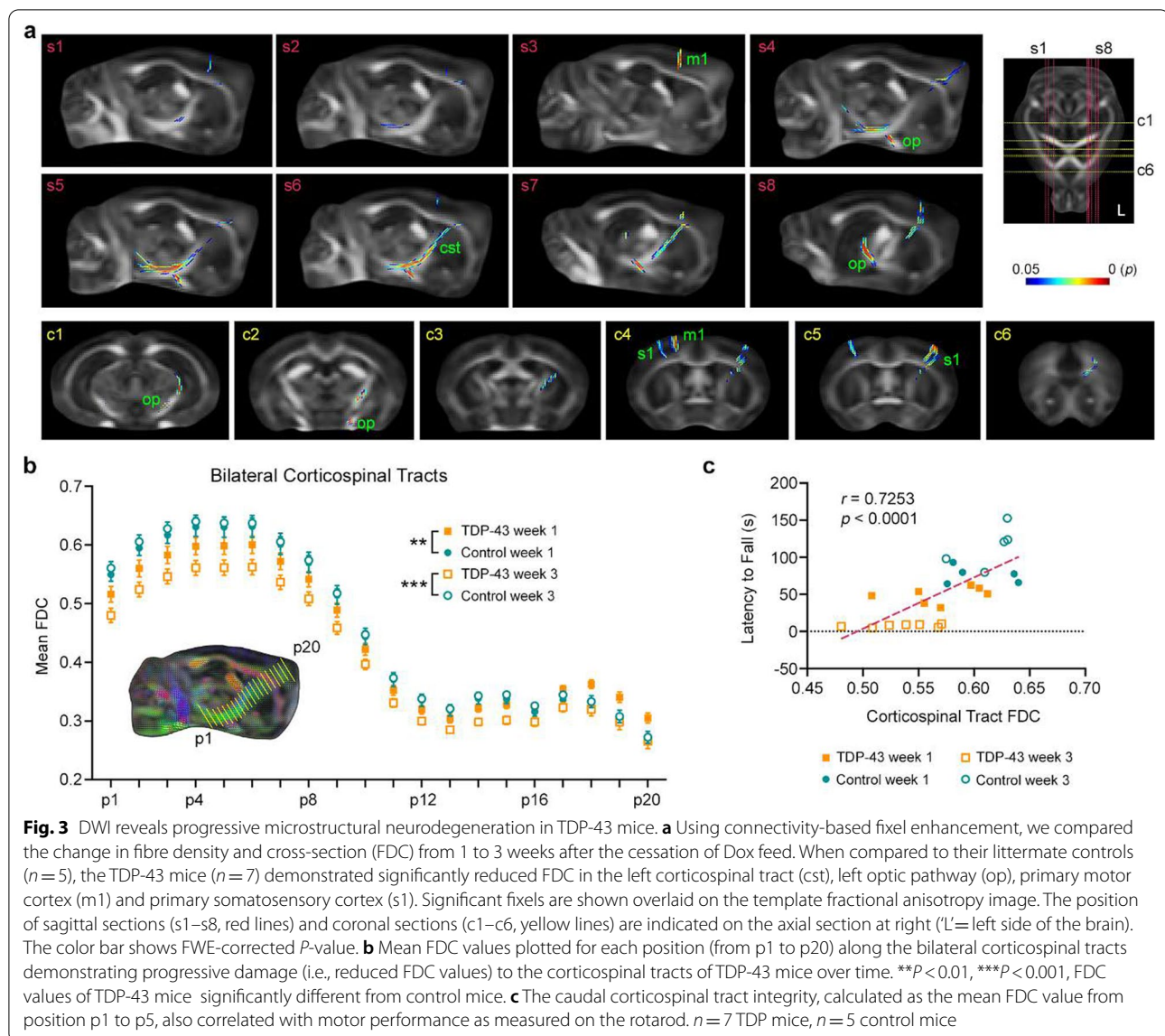
In addition to the exploratory analysis, we also performed a volumetric analysis of atlas-defined ROIs. Regions were selected a priori and included the neocortex, hypothesized to be the structure most likely to be affected early in the disease course [20], the hippocampus, the whole-brain, and the hypothalamus which contains the majority of orexin-producing neurons involved in wakefulness [21]. Two-way ANOVA revealed significant genotype and time interactions for volumes of both the neocortex ($F_{1,10} = 20.29$, $P = 0.0011$; Fig. 2b) and hippocampus ($F_{1,10} = 7.53$, $P = 0.0207$; Fig. 2c). No differences were observed between TDP-43 and control mice at 1 or 3 weeks post-Dox feed using Šídák's multiple comparison testing. No significant differences were found for the whole brain (Fig. 2d) or the hypothalamus (Fig. 2e).

In vivo DWI demonstrated microstructural white matter changes in the brains of TDP-43 mice

DWI methods can detect microstructural changes to the white matter in the absence of any macroscopic changes on conventional structural images [22, 23]. Using multi-tissue constrained spherical deconvolution,

we estimated a fibre orientation distribution for each voxel. Unlike DTI-derived metrics, which contain contributions from multiple fibre bundles in each voxel (often orientated in different directions), constrained spherical deconvolution allows diffusion metrics to be extracted for each *fixel* (i.e. individual fibre bundles within each voxel). Further, these metrics can be tested using fixel-based analysis to localize changes to individual fibre bundles and are therefore less likely to be confounded by crossing fibre bundles.

We compared the change in white matter connectivity (i.e., Δ FDC) between TDP-43 mice and control mice using connectivity-based fixel enhancement (Fig. 3). Results showed significantly greater Δ FDC in TDP-43 mice over time. The affected fibre bundles included the left corticospinal tract (Fig. 3a, panels s4–s7) and left optic pathway (Fig. 3a, panels s4 to s8, and c1 and c2). The left and right cortices were also affected, including fibres in the primary motor cortex and primary somatosensory cortex (hindlimb and forelimb regions, Fig. 3a, panels c4 and c5), with TDP-43 mice demonstrating significantly greater Δ FDC between 1 and 3 weeks post-Dox.



As corticospinal tract degeneration is a feature of ALS [13, 24, 25], we also performed an a priori analysis of these white matter fibre bundles. Corticospinal tract fixels demonstrated a progressive reduction in FDC values in TDP-43 mice compared to controls. We measured FDC values at 20 equidistant points (p1, p2, ..., p20) along the left and right corticospinal tracts. For each point, we then calculated the average FDC value from both hemispheres. There was a significant interaction between genotype and time ($F_{1,200} = 202.655$, $P < 0.001$, Wilks' $\Lambda = 0.497$), with the TDP-43 mice having significantly decreased FDC at both 1 and 3 weeks post-Dox ($P = 0.001$ and $P < 0.001$, respectively). Although there was no interaction for either time \times position or time \times position \times genotype, visual

inspection of the mean FDC values showed that the FDC decrease occurred at the caudal end of the corticospinal tract (Fig. 3b).

Finally, we investigated whether the observed corticospinal tract degeneration (i.e., average FDC values along the caudal section) correlated with the deteriorating motor deficits (i.e., latency to fall). Results showed that the mean FDC values correlated with the latency to fall ($r_{22} = 0.7253$, $P < 0.0001$) and this correlation also held true within the TDP-43 mice only ($r_{12} = 0.5561$, $P = 0.0389$) (Fig. 3c).

DCE-MRI revealed altered glymphatic clearance in symptomatic TDP-43 mice

Following in vivo MRI assessments of brain morphology and white matter degeneration, we assessed

glymphatic clearance using DCE-MRI. Cisterna magna cannulation, infusion of MR contrast agent and DCE-MRI were successfully performed in five TDP-43 mice and five control mice. Two mice were removed due to experimental error that resulted in no contrast agent administration. T_1 -weighted images demonstrated clear differences between the two groups (Fig. 4a). A delay in acquiring images in one TDP-43 mouse resulted in a single missing datapoint, and therefore statistical testing was performed using a mixed-effect analysis.

The signal increase from baseline, expressed as a percentage, was analyzed for six ROIs. In all cases, statistical testing revealed a main effect of post-infusion time, with $P < 0.0001$ for each. Over the whole brain (excluding the ventricles), a significant genotype and time interaction ($F_{17,135} = 3.38$, $P < 0.0001$) and a significant effect of genotype ($F_{1,8} = 16.39$, $P = 0.0037$) were observed (Fig. 4b). Ventral brain regions including the pons (Fig. 4c) and amygdala (Fig. 4d) exhibited a similar response over time,

with significantly increased signal intensity in TDP-43 mice compared to their littermate controls. Mixed-effect analyses demonstrated significant genotype and time interactions ($F_{17,135} = 5.83$, $P < 0.0001$ and $F_{17,135} = 15.52$, $P < 0.0001$, respectively) as well as significant effects of genotype ($F_{1,8} = 22.95$, $P = 0.0014$ and $F_{1,8} = 23.00$, $P = 0.0014$, respectively). In the cerebellum (Fig. 4e), a significant interaction between genotype and post-infusion time was also recorded ($F_{17,135} = 5.75$, $P < 0.0001$), with a main effect of genotype ($F_{1,8} = 5.84$, $P < 0.0420$).

The percent signal change from baseline in the thalamus was significantly different between TDP-43 and control mice (Fig. 4f). In contrast to the control mice that showed almost no increase from baseline, the TDP-43 mice showed gradual increase in signal, peaking at ~100 min after contrast agent administration. Mixed-effect analysis revealed a significant interaction between genotype and post-infusion time ($F_{17,135} = 3.21$, $P < 0.0001$) and a significant main effect of genotype

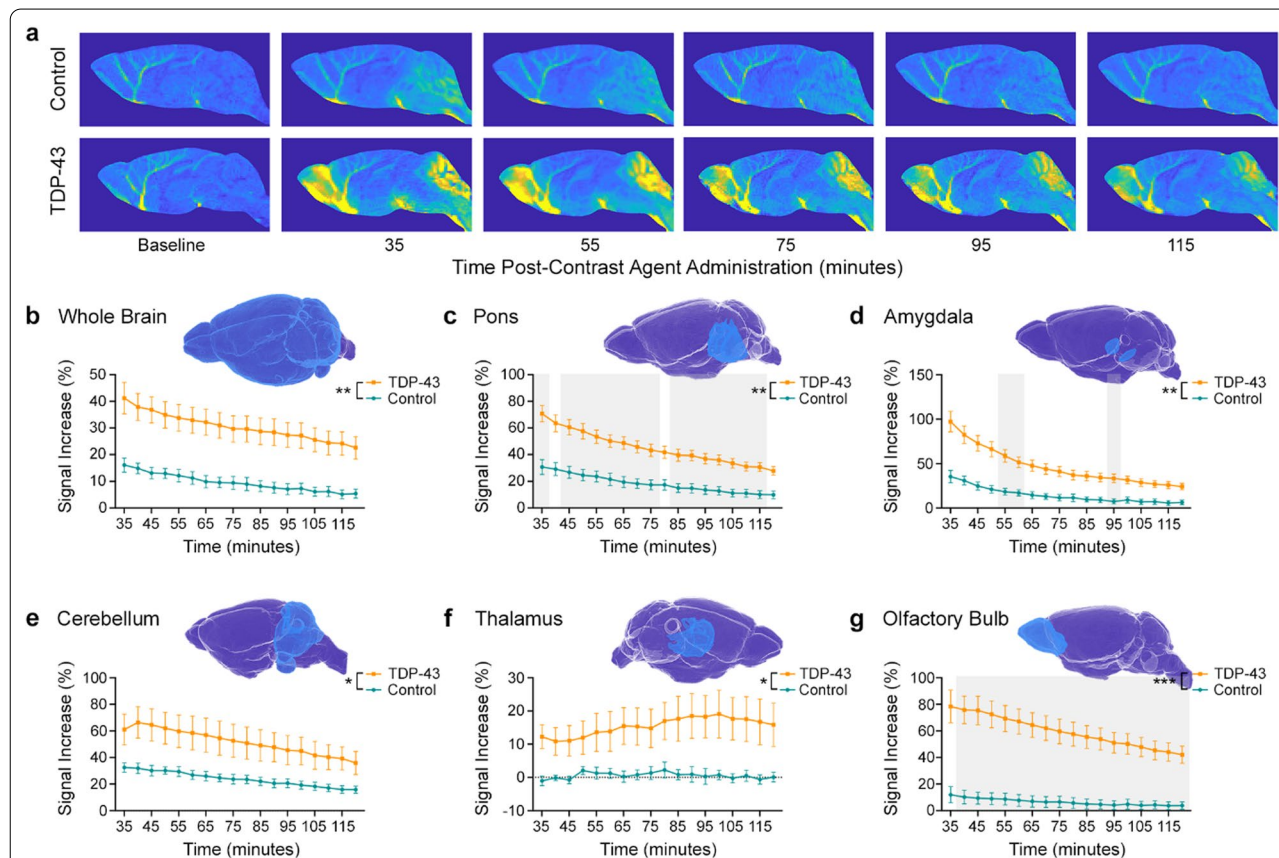


Fig. 4 Dynamic contrast-enhanced MRI (DCE-MRI) revealed impaired glymphatic clearance in TDP-43 mice. **a** Representative DCE-MRI images of control (top row) and TDP-43 (bottom row) mice over time after contrast agent administration. **b–g** Percent signal increase from baseline in the whole brain, pons, amygdala, cerebellum, thalamus and olfactory bulb. In all cases, mixed-effect analysis revealed a significant interaction between genotype and post-infusion time and main effects of both genotype ($*P < 0.05$, $**P < 0.01$, $***P < 0.001$) and time. Each atlas-defined ROI is shown in blue above the corresponding graph. Grey backgrounds in panels **c**, **d**, and **g** indicate times for which multiple comparison testing demonstrated significant differences between TDP-43 mice ($n = 5$) and their littermate controls ($n = 5$)

($F_{1,8}=5.98$, $P<0.0402$). Finally, the olfactory bulb (Fig. 4g) also demonstrated a significant interaction between genotype and post-infusion time ($F_{17,135}=22.98$, $P<0.0001$), and a main effect of genotype ($F_{1,8}=31.08$, $P<0.0005$).

Post-mortem investigations revealed reduced muscle mass and shorter telomere length in TDP-43 mice

Following DCE-MRI, the mice were sacrificed, and the gastrocnemius muscles (TDP $n=7$, control $n=5$) and spleens were collected and weighed (Fig. 5a–c). The right gastrocnemius muscles from the TDP-43 mice were significantly lighter than those from littermate controls ($t_{10}=5.10$, $P=0.0005$). TDP-43 mice also had a trend ($t_{10}=1.88$, $P=0.0903$) for smaller spleens than their littermate controls (Fig. 5c). The spleen weight (mean \pm SEM) was 70.2 ± 5.18 mg for control mice and 59.29 ± 3.28 mg for TDP-43 mice.

As conjecture remains surrounding how telomeres are affected in ALS, we also assessed telomere length using quantitative PCR on DNA extracted from ear tissue samples (Fig. 5d). Unpaired t -test analysis revealed that the TDP-43 mice ($n=6$) had significantly shorter telomeres ($t_8=4.26$, $P=0.0028$) than their littermate controls ($n=4$). The telomere length (mean \pm SEM) was 5593 ± 103.5 bp for control mice and 4784 ± 137.3 bp for the TDP-43 mice.

Discussion

In this study, we assessed glymphatic function in a transgenic mouse model with Dox-suppressible expression of hTDP-43. The mice were removed from Dox feed to permit hTDP-43 expression, then they were assessed longitudinally using rotarod testing and underwent in vivo multimodal MRI followed by DCE-MRI at 3 weeks post-Dox cessation. Our results demonstrate that the TDP-43 mice exhibited significantly altered glymphatic

function, progressive neurodegeneration, deteriorating motor symptoms, significant weight loss, and shortened telomere length when compared to their littermate controls, very early in the disease course.

Waste protein inclusions are a hallmark of all neurodegenerative diseases and recent efforts have recognized the importance of the glymphatic system for protein regulation and brain clearance. This brain-wide network of perivascular space facilitates the exchange of CSF and interstitial fluid, clearing waste from the CSF while also assisting in distributing compounds critical to neurological function. Here, we used DCE-MRI to investigate glymphatic function following the injection of an MR contrast agent, Magnevist, into the cisterna magna, a technique first demonstrated by Iliff and colleagues [12].

As hypothesized, glymphatic function was found to be altered in TDP-43 mice at 3 weeks post-Dox cessation, a time point prior to overt neurodegeneration (4 weeks) and very early in the disease course in this model [11]. Although this is the first in vivo study of glymphatic function in ALS and one of the few DCE-MRI studies conducted in mice, similar results demonstrating increased signal with impaired glymphatic function have been observed in rodents previously [26, 27]. One recent study employed DCE-MRI to investigate the effect of the circadian light/dark cycle in awake rats [28]. This study also showed similar brain-wide kinetics, with increased signal during the dark (awake) phase—when glymphatic clearance is known to be reduced. Although we did not acquire images during contrast agent infusion and hence were unable to similarly quantify the time to peak signal increase, we demonstrated significant interactions between time and genotype for each of the regions analyzed, and further, found a delay in contrast agent uptake in the thalamus, suggesting impaired glymphatic function in TDP-43 mice.

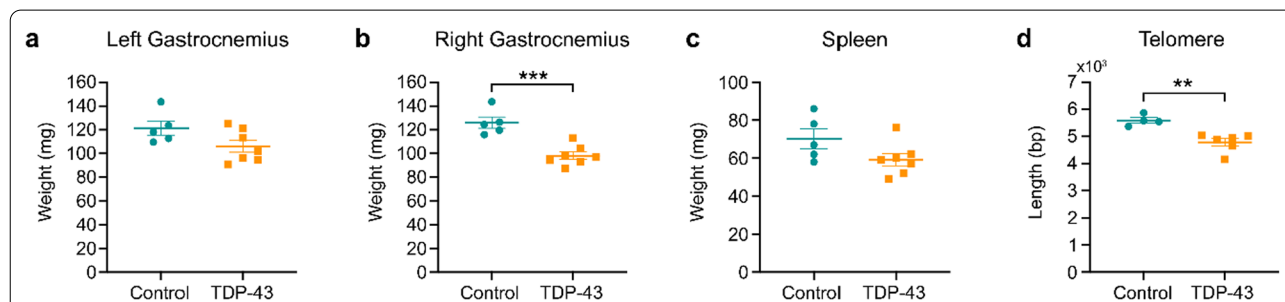


Fig. 5 Post-mortem analyses revealed muscle atrophy and reduced telomere length in TDP-43 mice. **a, b** Although not reaching significance on the left-side, the right-side gastrocnemius muscles were significantly lighter in TDP-43 mice ($n=7$) when compared to control mice ($n=5$) at 3 weeks after the cessation of Dox feed. **c** TDP-43 mice also tended to have lighter spleens. **d** Telomere length was assessed using quantitative PCR on DNA extracted from ear tissue samples and found to be significantly shorter in TDP-43 mice ($n=6$) when compared to control mice ($n=4$). ** $P<0.01$, *** $P<0.001$

Our preliminary results highlight the need for additional experiments, at multiple time points, to improve our understanding of the relationship between ALS and glymphatic system function, and how this relationship evolves with disease progression. In addition to measuring signal change during contrast agent infusion for the spatial quantification of measures such as peak signal increase and the time to peak signal increase, future experiments should also consider the use of α_2 agonists such as xylazine and dexmedetomidine [29, 30]. When compared to isoflurane alone, dexmedetomidine and low-dose isoflurane significantly increased glymphatic transport [30] and the interstitial fluid space [31] and hence, may better mimic sleep [32].

In addition to DCE-MRI, we performed in vivo MRI at 1 and 3 weeks after the cessation of Dox feed. Structural analysis of hippocampal volume demonstrated an interaction between genotype and time, with volumes increasing in control mice and decreasing over time in TDP-43 mice. Further, tensor-based morphometry also revealed atrophy of the hippocampus at 3 weeks post-Dox cessation. Altogether, these results suggest a possible loss of hippocampus neurons in TDP-43 mice over time. Hippocampal pathology is well documented in ALS patients primarily at later stages of disease [3, 20, 33–35] and a recent experimental study also demonstrated significant neuronal loss and atrophy of the hippocampus, after intracranial injection of recombinant adeno-associated virus serotype 9 containing human wild-type TDP-43, into the hippocampus of *CAMKII-tTa* transgenic mice [36]. Expression of a C-terminal fragment of TDP-43 found in the brains of frontotemporal lobar degeneration cases, has also been shown to cause a specific loss of hippocampal dentate gyrus neurons in mice, although the relevance for this finding to ALS remains unclear [37].

DWI has demonstrated potential as a sensitive biomarker for neurodegeneration, identifying microstructural changes to the white matter in the absence of any macroscopic changes on conventional radiological images [22, 23]. We assessed the fixel-derived metric FDC using both exploratory whole-brain and a priori analyses. As the name suggests, changes in the combined fibre density and cross-section measure reflect both a macroscopic change to the white matter bundle and a microstructural change due to increased or decreased axon fibre population [15, 38]. Further, as a fixel-derived metric, FDC can be assessed for specific fibre bundle orientations and hence, specific white matter tracts of interest.

The corticospinal tract is the major neuronal pathway controlling movement and has previously been implicated in DWI studies of ALS [13, 24, 25, 39]. Using connectivity-based fixel analysis, a whole-brain exploratory

method, we found significantly reduced FDC in the left corticospinal tract of TDP-43 mice over time. Additionally, hypothesis-driven tract-of-interest analyses of bilateral corticospinal tract FDC values also demonstrated significant reductions in TDP-43 mice compared to littermate controls. Post-hoc comparisons demonstrated that the TDP-43 mice had significantly reduced FDC in the corticospinal tracts at 1 week post-Dox cessation, largely at the caudal end, near the cerebral peduncles. These changes were observed in the absence of any structural change to the primary motor cortices on T_2^* -weighted imaging, consistent with the hypothesis that axonopathy may precede the degeneration of neuronal cell bodies—i.e. ‘dying-back pathology’ [19, 40–42].

Consistent with the progressive corticospinal tract degeneration and the ALS phenotype, the TDP-43 mice also demonstrated progressive weight loss and deteriorating motor deficits when compared to controls. The motor performance of TDP-43 mice was significantly impaired compared to controls at 1 week post-Dox cessation, with over half also demonstrating a hind-limb clasping phenotype. At 3 weeks post-Dox cessation, clasping was evident in all TDP-43 mice and motor performance had further declined. Interestingly, the rotarod latency to fall correlated significantly with the mean caudal corticospinal tract FDC values, suggesting that the decline of motor function is closely associated with corticospinal tract degeneration.

As expected, the gastrocnemii weight of TDP-43 mice was significantly lighter than that of littermate controls. Post-mortem analysis also demonstrated a trend of smaller spleens in these mice, consistent with observations of reduced spleen weight late in the disease course in *SOD1^{G93A}* mice [43, 44]. Peripheral immune dysfunction is a pathogenic feature of clinical ALS, with altered levels of T-lymphocytes, monocytes and cytokines in the blood [45], and it is possible that similar immune system changes may occur in this TDP-43 mouse model.

Chronic systemic inflammation and immune cell exhaustion are also hypothesized sources of telomere shortening [46]. Telomeres are special chromatin structures formed at the ends of chromosomes, protecting them from degradation and recombination [47]. Each time a cell divides, the telomeres shorten, and hence telomere length is considered a measure of ageing [47]. Telomere shortening has been reported in other neurodegenerative diseases, including traumatic brain injury [17, 48, 49] and Alzheimer’s disease [50, 51]. Consistent with this, we found that telomere length was significantly shorter in TDP-43 mice when compared to controls.

In both sporadic ALS patients and healthy controls, telomere length has been shown to correlate with decreased telomerase reverse transcriptase expression

[52]. In addition to maintaining telomere length, telomerase may also protect against cell damage. Increasing telomerase expression has been shown to delay disease onset in SOD1^{G93A} mice [53], while conversely, telomerase deletion accelerates disease progression in SOD1^{G93A} mice [54]. These results, together with our observation of reduced telomere length in TDP-43 mice, suggest telomere/telomerase dysfunction in the pathogenesis of ALS.

Conclusions

In conclusion, we demonstrate that when compared to their littermate controls, the TDP-43 mice exhibit progressive neurodegeneration including that within the corticospinal tract that correlates with deteriorating motor symptoms, significant weight loss including muscle atrophy, and shortened telomere length—outcomes consistent with an ALS-like phenotype. Furthermore, we have shown that in the presence of this phenotype, these mice have significantly disrupted glymphatic function. While the relationship between glymphatic clearance and ALS disease progression remains to be elucidated, given that these changes occur very early in the disease course in the TDP-43 mice, these results provide initial evidence to suggest that, like other neurodegenerative disorders, the glymphatic system could be a potential therapeutic target in the treatment of ALS.

Abbreviations

ALS: Amyotrophic lateral sclerosis; CSF: Cerebrospinal fluid; DCE-MRI: Dynamic contrast-enhanced magnetic resonance imaging; Dox: Doxycycline; DWI: Diffusion-weighted imaging; FDC: Fibre density and cross-section; FWE: Family-wise error; MRI: Magnetic resonance imaging; ROI: Region of interest; TDP-43: Transactive response DNA-binding protein 43; NEFH: Neurofilament heavy chain; TE: Echo time; TR: Repetition time; SEM: Standard error of the mean.

Acknowledgements

The authors acknowledge the facilities and scientific and technical assistance of the National Imaging Facility (NIF), a National Collaborative Research Infrastructure Strategy (NCRIS) capability at Monash Biomedical Imaging (MBI), a Technology Research Platform at Monash University.

Authors' contributions

AZ and DKW conceptualized and designed the study, collected data and performed analyses. DKW prepared the initial draft of the manuscript and prepared all figures. All authors read and approved the final manuscript.

Funding

This work was supported by the National Health and Medical Research Council to DKW (1174040) and AW (1140386), the Ross Maclean Fellowship and Brazil Family Program for Neurology to AW, and a Bethlehem Griffiths Research Foundation Grant to AZ, AW, and DKW (BGRF2103). The funding bodies did not take part in design of the study, nor the collection, analysis, interpretation of data or writing of the manuscript.

Availability of data and materials

The datasets used and/or analysed during the current study are available from the corresponding author on reasonable request.

Declarations

Ethics approval and consent to participate

All experimental procedures were approved by the Alfred Research Alliance Animal Ethics Committee (E/1997/2020/M) and the University of Queensland Animal Ethics Committee (QBI/040/18) and complied with the guidelines of the Australian Code of Practice for the Care and Use of Animals for Scientific Purposes.

Consent for publication

Not applicable.

Competing interests

The authors declare that they have no competing interests.

Author details

¹Department of Neuroscience, Central Clinical School, Monash University, Melbourne, VIC 3004, Australia. ²Queensland Brain Institute, The University of Queensland, St Lucia, QLD 4072, Australia. ³The Murdoch Children's Research Institute, The Royal Children's Hospital, Parkville, VIC 3052, Australia. ⁴Department of Pediatrics, The University of Melbourne, Parkville, VIC 3052, Australia. ⁵Department of Medicine, The Royal Melbourne Hospital, The University of Melbourne, Parkville, VIC 3052, Australia.

Received: 8 December 2021 Accepted: 17 February 2022

Published online: 15 March 2022

References

- Soto C, Pritzkow S. Protein misfolding, aggregation, and conformational strains in neurodegenerative diseases. *Nat Neurosci*. 2018;21(10):1332–40.
- Cohen TJ, Lee VM, Trojanowski JQ. TDP-43 functions and pathogenic mechanisms implicated in TDP-43 proteinopathies. *Trends Mol Med*. 2011;17(11):659–67.
- Neumann M, Sampathu DM, Kwong LK, Truax AC, Micsenyi MC, Chou TT, et al. Ubiquitinated TDP-43 in frontotemporal lobar degeneration and amyotrophic lateral sclerosis. *Science*. 2006;314(5796):130–3.
- Mishra PS, Boutej H, Soucy G, Bareil C, Kumar S, Picher-Martel V, et al. Transmission of ALS pathogenesis by the cerebrospinal fluid. *Acta Neuropathol Commun*. 2020;8(1):65.
- Hergesheimer RC, Chami AA, de Assis DR, Vourc'h P, Andres CR, Corcia P, et al. The debated toxic role of aggregated TDP-43 in amyotrophic lateral sclerosis: a resolution in sight? *Brain*. 2019;142(5):1176–94.
- Porta S, Xu Y, Restrepo CR, Kwong LK, Zhang B, Brown HJ, et al. Patient-derived frontotemporal lobar degeneration brain extracts induce formation and spreading of TDP-43 pathology in vivo. *Nat Commun*. 2018;9(1):4220.
- Iliff JJ, Wang M, Liao Y, Plogg BA, Peng W, Gundersen GA, et al. A paravascular pathway facilitates CSF flow through the brain parenchyma and the clearance of interstitial solutes, including amyloid beta. *Sci Transl Med*. 2012;4(147):147ra11.
- Kress BT, Iliff JJ, Xia M, Wang M, Wei HS, Zeppenfeld D, et al. Impairment of paravascular clearance pathways in the aging brain. *Ann Neurol*. 2014;76(6):845–61.
- Boentert M. Sleep disturbances in patients with amyotrophic lateral sclerosis: current perspectives. *Nat Sci Sleep*. 2019;11:97–111.
- Shokri-Kojori E, Wang GJ, Wiers CE, Demiral SB, Guo M, Kim SW, et al. beta-Amyloid accumulation in the human brain after one night of sleep deprivation. *Proc Natl Acad Sci U S A*. 2018;115(17):4483–8.
- Walker AK, Spiller KJ, Ge G, Zheng A, Xu Y, Zhou M, et al. Functional recovery in new mouse models of ALS/FTLD after clearance of pathological cytoplasmic TDP-43. *Acta Neuropathol*. 2015;130(5):643–60.
- Iliff JJ, Lee H, Yu M, Feng T, Logan J, Nedergaard M, et al. Brain-wide pathway for waste clearance captured by contrast-enhanced MRI. *J Clin Invest*. 2013;123(3):1299–309.

13. Wright DK, Liu S, van der Poel C, McDonald SJ, Brady RD, Taylor L, et al. Traumatic brain injury results in cellular, structural and functional changes resembling motor neuron disease. *Cereb Cortex*. 2017;27(9):4503–15.
14. Tournier JD, Smith R, Raffelt D, Tabbara R, Dhollander T, Pietsch M, et al. MRtrix3: A fast, flexible and open software framework for medical image processing and visualisation. *Neuroimage*. 2019;202:116137.
15. Raffelt DA, Tournier JD, Smith RE, Vaughan DN, Jackson G, Ridgway GR, et al. Investigating white matter fibre density and morphology using fixel-based analysis. *Neuroimage*. 2017;144(Pt A):58–73.
16. Mychasiuk R, Hehar H, Ma I, Esser MJ. Dietary intake alters behavioral recovery and gene expression profiles in the brain of juvenile rats that have experienced a concussion. *Front Behav Neurosci*. 2015;9:17.
17. Wright DK, O'Brien TJ, Mychasiuk R, Shultz SR. Telomere length and advanced diffusion MRI as biomarkers for repetitive mild traumatic brain injury in adolescent rats. *Neuroimage Clin*. 2018;18:315–24.
18. Smith SM, Nichols TE. Threshold-free cluster enhancement: addressing problems of smoothing, threshold dependence and localisation in cluster inference. *Neuroimage*. 2009;44(1):83–98.
19. White MA, Lin Z, Kim E, Henstridge CM, Pena Altamira E, Hunt CK, et al. Sarm1 deletion suppresses TDP-43-linked motor neuron degeneration and cortical spine loss. *Acta Neuropathol Commun*. 2019;7(1):166.
20. Braak H, Brettschneider J, Ludolph AC, Lee VM, Trojanowski JQ, Del Tredici K. Amyotrophic lateral sclerosis—a model of corticofugal axonal spread. *Nat Rev Neurol*. 2013;9(12):708–14.
21. Kang JE, Lim MM, Bateman RJ, Lee JJ, Smyth LP, Cirrito JR, et al. Amyloid-beta dynamics are regulated by orexin and the sleep-wake cycle. *Science*. 2009;326(5955):1005–7.
22. Wright DK, Symons GF, O'Brien WT, McDonald SJ, Zamani A, Major B, et al. Diffusion imaging reveals sex differences in the white matter following sports-related concussion. *Cereb Cortex*. 2021;31:4411.
23. Wright DK, Trezise J, Kamnakh A, Bekdash R, Johnston LA, Ordidge R, et al. Behavioral, blood, and magnetic resonance imaging biomarkers of experimental mild traumatic brain injury. *Sci Rep*. 2016;6:28713.
24. Raffelt D, Tournier JD, Rose S, Ridgway GR, Henderson R, Crozier S, et al. Apparent fibre density: a novel measure for the analysis of diffusion-weighted magnetic resonance images. *Neuroimage*. 2012;59(4):3976–94.
25. Raffelt DA, Smith RE, Ridgway GR, Tournier JD, Vaughan DN, Rose S, et al. Connectivity-based fixel enhancement: whole-brain statistical analysis of diffusion MRI measures in the presence of crossing fibres. *Neuroimage*. 2015;117:40–55.
26. Jiang Q, Zhang L, Ding G, Davoodi-Bojd E, Li Q, Li L, et al. Impairment of the glymphatic system after diabetes. *J Cereb Blood Flow Metab*. 2017;37(4):1326–37.
27. Gaberel T, Gakuba C, Goulay R, De Lizarrondo SM, Hanouz JL, Emery E, et al. Impaired glymphatic perfusion after strokes revealed by contrast-enhanced MRI: a new target for fibrinolysis? *Stroke*. 2014;45(10):3092–6.
28. Cai X, Qiao J, Kulkarni P, Harding IC, Ebong E, Ferris CF. Imaging the effect of the circadian light-dark cycle on the glymphatic system in awake rats. *Proc Natl Acad Sci U S A*. 2020;117(1):668–76.
29. Hablitz LM, Vinitsky HS, Sun Q, Staeger FF, Sigurdsson B, Mortensen KN, et al. Increased glymphatic influx is correlated with high EEG delta power and low heart rate in mice under anesthesia. *Sci Adv*. 2019;5(2):eaav5447.
30. Benveniste H, Lee H, Ding F, Sun Q, Al-Bizri E, Makaryus R, et al. Anesthesia with dexmedetomidine and low-dose isoflurane increases solute transport via the glymphatic pathway in rat brain when compared with high-dose isoflurane. *Anesthesiology*. 2017;127(6):976–88.
31. Ozturk BO, Monte B, Koundal S, Dai F, Benveniste H, Lee H. Disparate volumetric fluid shifts across cerebral tissue compartments with two different anesthetics. *Fluids Barriers CNS*. 2021;18(1):1.
32. Xie L, Kang H, Xu Q, Chen MJ, Liao Y, Thiyagarajan M, et al. Sleep drives metabolite clearance from the adult brain. *Science*. 2013;342(6156):373–7.
33. Abdulla S, Machts J, Kaufmann J, Patrick K, Kollwe K, Dengler R, et al. Hippocampal degeneration in patients with amyotrophic lateral sclerosis. *Neurobiol Aging*. 2014;35(11):2639–45.
34. Takeda T, Uchihara T, Arai N, Mizutani T, Iwata M. Progression of hippocampal degeneration in amyotrophic lateral sclerosis with or without memory impairment: distinction from Alzheimer disease. *Acta Neuropathol*. 2009;117(1):35–44.
35. Westeneng HJ, Verstraete E, Walhout R, Schmidt R, Hendrikse J, Veldink JH, et al. Subcortical structures in amyotrophic lateral sclerosis. *Neurobiol Aging*. 2015;36(2):1075–82.
36. Quadri Z, Johnson N, Zamudio F, Miller A, Peters M, Smeltzer S, et al. Overexpression of human wtTDP-43 causes impairment in hippocampal plasticity and behavioral deficits in CAMKII-tTa transgenic mouse model. *Mol Cell Neurosci*. 2020;102:103418.
37. Walker AK, Tripathy K, Restrepo CR, Ge G, Xu Y, Kwong LK, et al. An insoluble frontotemporal lobar degeneration-associated TDP-43 C-terminal fragment causes neurodegeneration and hippocampus pathology in transgenic mice. *Hum Mol Genet*. 2015;24(25):7241–54.
38. Mito R, Raffelt D, Dhollander T, Vaughan DN, Tournier JD, Salvado O, et al. Fibre-specific white matter reductions in Alzheimer's disease and mild cognitive impairment. *Brain*. 2018;141(3):888–902.
39. Cheng L, Tang X, Luo C, Liu D, Zhang Y, Zhang J. Fiber-specific white matter reductions in amyotrophic lateral sclerosis. *Neuroimage Clin*. 2020;28:102516.
40. Krauss R, Bosanac T, Devraj R, Engber T, Hughes RO. Axons matter: the promise of treating neurodegenerative disorders by targeting SARM1-mediated axonal degeneration. *Trends Pharmacol Sci*. 2020;41(4):281–93.
41. Fischer LR, Culver DG, Tennant P, Davis AA, Wang M, Castellano-Sanchez A, et al. Amyotrophic lateral sclerosis is a distal axonopathy: evidence in mice and man. *Exp Neurol*. 2004;185(2):232–40.
42. Nair G, Carew JD, Usher S, Lu D, Hu XP, Benatar M. Diffusion tensor imaging reveals regional differences in the cervical spinal cord in amyotrophic lateral sclerosis. *Neuroimage*. 2010;53(2):576–83.
43. Pollari E, Savchenko E, Jaronen M, Kanninen K, Malm T, Wojciechowski S, et al. Granulocyte colony stimulating factor attenuates inflammation in a mouse model of amyotrophic lateral sclerosis. *J Neuroinflammation*. 2011;8:74.
44. Banerjee R, Mosley RL, Reynolds AD, Dhar A, Jackson-Lewis V, Gordon PH, et al. Adaptive immune neuroprotection in G93A-SOD1 amyotrophic lateral sclerosis mice. *PLoS One*. 2008;3(7):e2740.
45. McCombe PA, Lee JD, Woodruff TM, Henderson RD. The peripheral immune system and amyotrophic lateral sclerosis. *Front Neurol*. 2020;11:279.
46. Eitan E, Hutcheon ER, Mattson MP. Telomere shortening in neurological disorders: an abundance of unanswered questions. *Trends Neurosci*. 2014;37(5):256–63.
47. Blasco MA. Telomeres and human disease: ageing, cancer and beyond. *Nat Rev Genet*. 2005;6(8):611–22.
48. Symons GF, Clough M, O'Brien WT, Ernest J, Salberg S, Costello D, et al. Shortened telomeres and serum protein biomarker abnormalities in collision sport athletes regardless of concussion history and sex. *J Concussion*. 2020;4:2059700220975609.
49. Sun M, Brady RD, Casillas-Espinosa PM, Wright DK, Semple BD, Kim HA, et al. Aged rats have an altered immune response and worse outcomes after traumatic brain injury. *Brain Behav Immun*. 2019;80:536–50.
50. Scheller Madrid A, Rasmussen KL, Rode L, Frikke-Schmidt R, Nordestgaard BG, Bojesen SE. Observational and genetic studies of short telomeres and Alzheimer's disease in 67,000 and 152,000 individuals: a Mendelian randomization study. *Eur J Epidemiol*. 2020;35(2):147–56.
51. Scarabino D, Broggio E, Gambina G, Corbo RM. Leukocyte telomere length in mild cognitive impairment and Alzheimer's disease patients. *Exp Gerontol*. 2017;98:143–7.
52. De Felice B, Annunziata A, Fiorentino G, Manfellotto F, D'Alessandro R, Marino R, et al. Telomerase expression in amyotrophic lateral sclerosis (ALS) patients. *J Hum Genet*. 2014;59(10):555–61.
53. Eitan E, Tichon A, Gazit A, Gitler D, Slavov S, Priel E. Novel telomerase-increasing compound in mouse brain delays the onset of amyotrophic lateral sclerosis. *EMBO Mol Med*. 2012;4(4):313–29.
54. Linkus B, Wiesner D, Messner M, Karabatsiakis A, Scheffold A, Rudolph KL, et al. Telomere shortening leads to earlier age of onset in ALS mice. *Aging*. 2016;8(2):382–93.